

# Searching For the Physical Drivers of Eigenvector 1: Influence of Black Hole Mass and Eddington Ratio

Paola Marziani<sup>1\*</sup>, Radoslav K. Zamanov<sup>1†</sup>, Jack W. Sulentic<sup>2</sup>, Massimo Calvani<sup>1</sup>

<sup>1</sup> *Istituto Nazionale di Astrofisica, Osservatorio Astronomico di Padova, Vicolo dell'Osservatorio 5, I-35122 Padova, Italy*

<sup>2</sup> *Department of Physics and Astronomy, University of Alabama, Tuscaloosa, AL 35487, USA*

Received .....; accepted .....

## ABSTRACT

We compute the virial mass of the central black hole ( $M$ ) and the luminosity-to-mass ( $L/M$ ) ratio of  $\approx 300$  low- $z$  quasars and luminous Seyfert 1 nuclei. We analyze: (1) whether radio-quiet and radio-loud objects show systematic differences in terms of  $M$  and  $L/M$ ; (2) the influence of  $M$  and  $L/M$  on the shape of the  $H\beta$  broad component line profile; (3) the significance of the so-called “blue outliers” i.e., sources showing a significant blueshift of the  $[OIII]\lambda\lambda 4959, 5007$  lines with respect to the narrow component of  $H\beta$  which is used as an estimator of the quasar reference frame. We show that  $M$  and  $L/M$  distributions for RQ and RL sources are likely different for samples matched in luminosity and redshift, in the sense that radio-quiet sources have systematically smaller masses and larger  $L/M$ . However, the  $L/M$  ratio distributions become indistinguishable if  $8.5 < \log M < 9.5$ . Line profile comparisons for median spectra computed over narrow ranges of  $M$  and  $L/M$  indicate that a Lorentz function provides a better fit for higher  $L/M$  sources and a double Gaussian for lower  $L/M$  values. A second (redshifted) Gaussian component at low  $L/M$  appears as a red asymmetry frequently observed in radio-loud and radio-quiet sources with broader ( $FWHM \gtrsim 4000$  km s<sup>-1</sup>)  $H\beta$  broad component profiles. This component becomes stronger in larger mass and lower  $L/M$  sources. No specific influence of radio loudness on the  $H\beta$  broad component profile is detected, although equivalent widths of  $H\beta$  broad component and especially of  $[OIII]\lambda\lambda 4959, 5007$  are larger for radio-loud sources. We identify five more “blue outlier” sources. Since these sources are, on average, one magnitude brighter than other AGNs with similar mass, they are accreting at an Eddington ratio that is 2-3 times higher. We hint at evolutionary effects that explain some of these results and reinforce the “Eigenvector 1” correlations.

**Key words:** quasars: emission lines – quasars: general – galaxies: active

## 1 INTRODUCTION

Studies of emission lines play an important role in our understanding of Active Galactic Nuclei (AGN) and the physics the accretion processes, although a connection between the main theoretical parameters (i.e., black hole mass, accretion rates, black hole spin, and a viewing angle) and observed spectral parameters is, at best, just sketchy and qualitative. In recent years, a major innovation has been ascribed to the so-called “Eigenvector 1” (E1) correlations (Boroson

& Green 1992). The original E1 was most closely related to the anti-correlation between  $Fe\ II_{opt}$  strength and peak  $[OIII]\lambda 5007$  intensity, and FWHM of the  $H\beta$  broad component ( $H\beta_{BC}$ ).

E1-related correlations have emerged as very robust, since they continue to appear in different low- $z$  AGN samples, even if a set of spectral parameters partly different from the ones used for the original Principal Component Analysis (PCA) by Boroson & Green (1992) is considered. An outstanding relationship in the context of E1 involves the  $FWHM(H\beta_{BC})$  and the ratio between the equivalent width of the  $Fe\ II_{opt}$  complex centered at  $\lambda 4570$  and  $H\beta_{BC}$ ,  $R_{FeII} = W(FeII\lambda 4570)/W(H\beta_{BC})$ . Low redshift AGN occupy an elbow sequence in the plane defined by these two parameters (see Sulentic et al. 2000a; Marziani et al. 2001). The overall sequence is defined by RQ sources while the RL AGN occupy only a restricted part of it. The domain

\* E-mail: marziani@pd.astro.it (PM); zamanov@pd.astro.it (RZ)  
calvani@pd.astro.it (MC), giacomo@merlot.astr.ua.edu (JWS)

† Present address: Astrophysics Research Institute, Liverpool John Moores University, Twelve Quays House, Egerton Wharf, Birkenhead CH41 1LD United Kingdom; email: rz@astro.livjm.ac.uk

where  $\text{FWHM}(\text{H}\beta_{\text{BC}}) \lesssim 4000 \text{ km s}^{-1}$  is predominantly occupied by RQ sources (Sulentic et al. 2000a; see also Sulentic et al. 2003). There is an apparent dichotomy in the  $\text{H}\beta_{\text{BC}}$  line profile shapes: sources with  $\text{FWHM}(\text{H}\beta_{\text{BC}}) \lesssim 4000 \text{ km s}^{-1}$  show typically a Lorentzian  $\text{H}\beta_{\text{BC}}$ , while for  $\text{FWHM}(\text{H}\beta_{\text{BC}}) \gtrsim 4000 \text{ km s}^{-1}$  a double Gaussian fit is more appropriate (Sulentic et al. 2002); (3) the so-called “blue outliers” (sources showing a significant blueshift of the  $[\text{OIII}]\lambda\lambda 4959, 5007$  lines with respect to inferred quasar frame) occur among sources with strongest  $\text{FeII}\lambda 4570$  narrowest  $\text{H}\beta_{\text{BC}}$  (Zamanov et al. 2002; Marziani et al. 2003a).

The robustness of the E1 correlations stems probably from a series of concurring factors: (1) an Eddington ratio that may be continuously changing along the E1 sequence (e.g., Boroson, Persson & Oke 1985; Boroson & Green 1992; Murray et al. 1995; Nicastro 2000; Marziani et al. 2001; Boroson 2002); (2) outflow/wind properties which are expected to depend on Eddington ratio (e.g., Dultzin-Hacyan et al. 2000; Marziani et al. 2001); (3) orientation effects that will blur any physical correlation and displace sources in the direction of increasing Eddington ratio (Marziani et al. 2001; see also, Nagao et al. 2000, Zhou et al. 2003); (4) Broad Line Region (BLR) structural effects (Sulentic et al. 2000b, Sulentic et al. 2002; see also the Proceeding of the Nebraska meeting for the E1 relevance for the Broad Line Region structure; Gaskell et al. 1999); (5) last, but not least, evolutionary effects that will lead to an increase of black hole mass as well as of the  $[\text{OIII}]\lambda 5007$  rest-frame equivalent width (Zamanov et al. 2002; Boroson 2002). We will briefly discuss them in § 8.4 and § 9.

Even if there is not yet a consensus (see e.g., Marziani et al. 2001; Boroson 2002), the physical drivers of E1 are likely to involve the luminosity-to-black hole mass ratio ( $L/M \propto$  Eddington ratio), an orientation angle, and the black hole mass ( $M$ ) (Zamanov & Marziani 2002). Additional properties such as black hole spin (e.g., Wilson & Colbert 1995) or the properties of the host galaxy environment (e.g., McLure et al. 1999) are also likely to play a role in any RQ-RL dichotomy.

This paper presents a basic investigation of the influence of  $L/M$  and  $M$  on RL and RQ sample properties, on the  $\text{H}\beta_{\text{BC}}$  line profile, and on the occurrence of the “blue outliers”, which are all major E1-dependent phenomena. In § 2 we present our quasar sample followed by (§ 3) derivation of  $M$  and  $L/M$ , (§ 4) presentation and discussion of mass – luminosity diagrams, (§ 5) a comparison of radio quiet and loud sources, (§ 6) an analysis of  $\text{H}\beta_{\text{BC}}$  profiles, (§ 7) as well as significance of the “blue outlier” sources. Our results are discussed in § 8. § 9 provides some concluding remarks.

## 2 SAMPLE DEFINITION & MEASUREMENTS

We use spectra of 278 AGNs. Our AGN sample includes 215 sources and has been presented elsewhere (Marziani et al. 2003b, hereafter M03). We added 63 soft X-ray selected sources with suitable optical spectroscopic data (Grupe et al. 1999; hereafter G99) because this turns out to be the most fertile source of “blue outliers”. Inclusion of Grupe et al. data makes our sample less biased, as described in §5.4. The optical characteristics of these X-ray selected sources include: (1) relatively “narrow” broad emission lines (e.g.

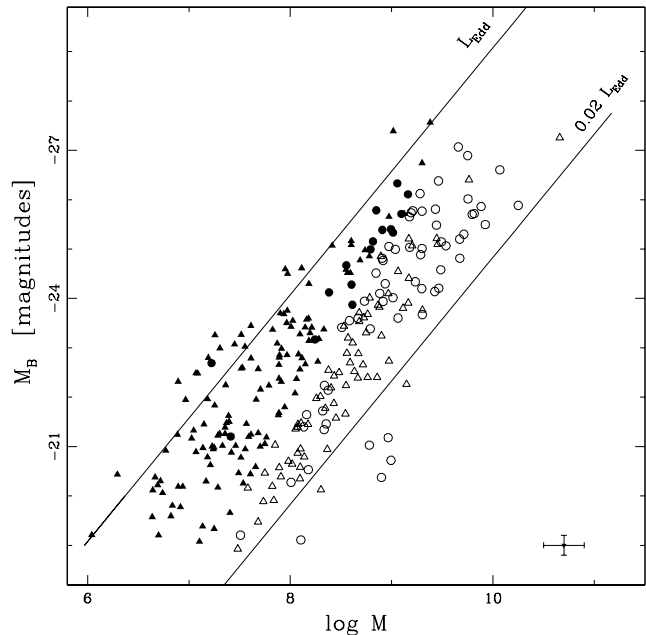


**Figure 1.** Distribution of absolute B magnitude ( $M_B$ ) versus black hole mass  $M$  (in solar units) for the 278 AGN sample.  $M_B$  values are corrected for the galactic extinction. Triangles and circles indicate radio-quiet and radio-loud sources respectively. Open symbols indicate sources with  $\text{FWHM}(\text{H}\beta_{\text{BC}}) \gtrsim 4000 \text{ km s}^{-1}$ ; filled symbols sources with  $\text{FWHM}(\text{H}\beta_{\text{BC}}) \lesssim 4000 \text{ km s}^{-1}$  (see §5.4). The bars in the lower right corner indicate typical errors.

Narrow Line Seyfert 1 [NLSy1] sources), (2) strong optical  $\text{Fe II}_{\text{opt}}$  blends and (3) weak forbidden emission lines. The merged datasets provide reasonable quality spectra ( $S/N \approx 20 - 70$ ) for the region near  $\text{H}\beta$  in 278 AGN ( $z \lesssim 0.8$ ). The M03 dataset is not complete (see M03 for discussion of completeness and sample biases).

We use line parameters reported in M03 and derive the corresponding measures (using the same procedures described in M03) for the X-ray selected sample from the digital spectra made publicly available by G99. We consider here measurements of the following parameters: (a)  $\text{FWHM}(\text{H}\beta_{\text{BC}})$ ; (b) equivalent width ratio  $R_{\text{FeII}} = W(\text{FeII}\lambda 4570) / W(\text{H}\beta_{\text{BC}})$ , (c)  $\text{FWHM}$  measurement of the lines in the  $\text{FeII}\lambda 4570$  blend (see M03 for details), (d) radial velocity difference between  $[\text{OIII}]\lambda 5007$  and  $\text{H}\beta$  at the line peak (without narrow component subtraction). Accuracy of the G99 wavelength calibration was evaluated by examining the distribution of radial velocity difference between  $[\text{OIII}]\lambda 4959$  and  $[\text{OIII}]\lambda 5007$ . Whenever possible,  $[\text{OIII}]\lambda 4363$  was also used and all inter-narrow line differences were found to be comparable to our measures (cf. Zamanov et al. 2002).

Apparent ( $m_V$ ), and absolute B magnitudes ( $M_B$ ) were taken from 10<sup>th</sup> edition of the AGN catalog (Véron-Cetty & Véron 2001). A magnitude correction  $+0.88 \text{ mag}$  was applied to convert  $M_B$  from  $H_0 = 50 \text{ km s}^{-1} \text{ Mpc}^{-1}$  to  $H_0 = 75 \text{ km s}^{-1} \text{ Mpc}^{-1}$  ( $q_0 = 0$ ) which we use throughout this paper. Galactic extinction values  $A_B$  were taken from NED following Schlegel et al. (1998). Sources were considered RL if the specific flux at 6 cm and in the B band was larger than

10, with data taken from the Véron-Cetty & Véron (2001) catalog.

### 3 COMPUTATION OF M AND L/M

#### 3.1 Black Hole Masses

One can estimate the mass of the putative supermassive black hole using  $\text{FWHM}(\text{H}\beta_{\text{BC}})$  and a reverberation “radius” (Kaspi et al. 2000) along with the assumption of virialized motions. It is now common to estimate the mass by assuming the BLR distance from the central continuum source  $r_{\text{BLR}} \propto (L_{5100})^\alpha$  and  $\alpha = 0.7$ , as derived from the reverberation data (Kaspi et al. 2000). The virial mass is  $M = r_{\text{BLR}} v^2 / G$ , where  $v = \sqrt{3}/2 \text{FWHM}(\text{H}\beta_{\text{BC}})$  (c.f. Woo & Urry 2002a), and  $G$  is the gravitational constant. We therefore can write the black hole virial mass as follows:

$$M = 4.817 \times \left( \frac{\text{FWHM}(\text{H}\beta_{\text{BC}})}{1 \text{ km s}^{-1}} \right)^2 \left( \frac{\lambda L_{5100}}{10^{44} \text{ erg s}^{-1}} \right)^{0.7}, \quad (1)$$

where  $M$  is in solar units,  $L_{5100}$  is the specific luminosity at  $5100 \text{ \AA}$  (in units of  $\text{ergs s}^{-1} \text{ cm}^{-2} \text{ \AA}^{-1}$ ), and

$$\lambda L_{5100} = 3.137 \times 10^{35-0.4(M_{\text{B}}-A_{\text{B}})} \text{ erg s}^{-1}. \quad (2)$$

In order to convert the absolute B magnitude  $M_{\text{B}}$  to  $\lambda L_{5100}$  we assumed that the specific flux is  $f_\nu \propto \nu^{-0.3}$ . The derived masses are thought to be reasonable estimates within a factor of about 2–3 (see also Woo & Urry 2002a, Vestergaard 2002).

#### 3.2 Influence of Orientation

Source viewing angle is especially important in AGN where the concepts of disk accretion/line emission and jet ejection are widely favored. In the above mass derivation formula we did not include any orientation related broadening factor. If  $\text{H}\beta_{\text{BC}}$  is emitted in a highly flattened structure then  $M$  can be underestimated by a factor  $\approx \sin i^{-2}$  in pole-on/face-on sources (i.e., with accretion disk axis oriented along our line of sight). Unfortunately, we do not yet have a proper way to estimate the viewing angle  $i$  for each source. This is a major drawback because there is observational evidence suggesting that orientation can affect line width by a factor  $\approx 2$  (Brotherton, 1996; Marziani et al. 2001; Jarvis & McLure, 2002). Even though we neglected the effects of orientation in the general sample population, we considered it in computations of  $M$  and  $L/M$  the relatively rare and extreme class that is likely observed close to “pole-on”: the “blue outliers” (§7.3).

#### 3.3 The Role of the BLR Size-Luminosity Relationship

The exponent in the relationship between source luminosity  $L$  and  $r_{\text{BLR}}$  is assumed to be  $\alpha = 0.7$ . Any deviation from this value has quantitative effects on our results. Our sample includes many moderately luminous quasars at  $0.4 < z < 0.8$ , so it is important to stress that the relationship derived by Kaspi et al. (2000) is based exclusively on quasars of  $z < 0.4$  and that the high (and low) luminosity ranges of the correlation are poorly sampled.

If we consider sources in the luminosity range  $43.4 \lesssim \log L/L_\odot \lesssim 45$  (i.e. where we have uniform luminosity sampling), the slope of the best fit is  $\alpha = 0.8$ , and could be easily as high as  $\alpha = 1$  without increasing significantly the fit standard deviation. Marziani et al. (2001) considered this case which seems appropriate for the PG quasar luminosity range. One must remain open to the possibility that  $0.5 \lesssim \alpha \lesssim 1$ , and that  $\alpha$  might even be a function of  $L$ . Changing  $\alpha$  implies an  $L$ -dependent change in mass estimates; therefore the slope of the luminosity-to-mass relationship (Fig. 1) is affected as well as the location of points in the  $L/M$  vs.  $M$  diagram (Fig. 7 & Fig. 12). Despite these possibilities, systematic trends discussed in this paper should not be affected.

#### 3.4 Bolometric Luminosity

We calculated the bolometric luminosity  $L$  from  $L \approx 10 \lambda L_\lambda(5100\text{\AA})$  (details can be found in Wandel, Peterson, & Malkan, 1999, Elvis et al. 1994, Collin et al. 2002). Values computed in this way were used to derive the  $L/M$  ratio. The  $L/M$  ratio everywhere is expressed in solar units with the solar value  $(L/M)_\odot = 1.92 \text{ ergs s}^{-1} \text{ g}^{-1}$ , and the Eddington limit corresponding to  $\log L/M = 4.53$ .

We neglected any possible differences in the spectral energy distribution between source subclasses. In order to test this benign neglect we considered 44 sources that are common with Woo and Urry (2002a) where SEDs were constructed from archival data. Comparison of our bolometric luminosity values showed no significant systematic difference:  $\overline{\Delta \log L} \approx -0.06$  for all 44 sources, with a standard deviation  $\sigma \approx 0.24$ . RQ sources show  $\overline{\Delta \log L} \approx -0.06$  with  $\sigma \approx 0.22$ , while RL  $\overline{\Delta \log L} \approx -0.07$  with a slightly larger  $\sigma \approx 0.26$ . If we consider separately RQ and RL sources with the restriction  $\text{FWHM}(\text{H}\beta_{\text{BC}}) \geq 4000 \text{ km s}^{-1}$  (see §5.3), we find  $\overline{\Delta \log L} \approx -0.05$  (RQ) and  $\overline{\Delta \log L} \approx -0.01$  (RL). It is worth noting that the scatter is due to a minority of bad-behaving data points ( $\approx 20\%$ ). If they are removed, the standard deviation becomes  $\sigma \approx 0.1$  in all cases, with systematic differences always  $\lesssim 0.05$ .

### 4 MASS - LUMINOSITY DIAGRAM

Fig.1 shows a plot of  $M_{\text{B}}$  vs.  $M$  for our combined sample which covers an absolute B magnitude range  $-20 \lesssim M_{\text{B}} \lesssim -27$  and an estimated black hole mass range  $10^7 \lesssim M \lesssim 10^{10}$  ( $M$  is everywhere given in  $M_\odot$ ). The data show a rather well-defined range in  $L/M$  with almost all sources lying between  $0.02 \lesssim L/L_{\text{Edd}} \lesssim 1.00$ . RQ sources show evidence for significant Malmquist bias while RL sources show the opposite trend probably related to a bias towards selecting higher luminosity core-dominated sources likely to be beamed.

### 5 RADIO LOUD AND RADIO QUIET AGN

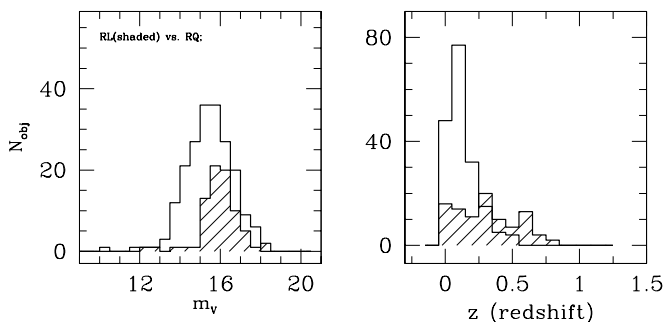
Table 1 presents average and median values of relevant properties for the RL and RQ subsamples. Kolmogorov-Smirnov tests indicate that RL and RQ samples differ significantly in redshift,  $m_V$  and absolute B magnitude distribution. The

**Table 1.** RQ/RL sample averages and medians for redshift, apparent V magnitude ( $m_V$ ), absolute B magnitude ( $M_B$ ), BH mass (M), and luminosity-to-mass ratio. Average values are given with sample standard deviations, median values with first and third quartile values.  $P_{KS}$  is the probability that the two distributions are randomly drawn from the same parent population using Kolmogorov-Smirnov tests.

	N	z			$m_V$			$M_B$		
		Aver. $\pm\sigma$	Med. <sub>25%</sub> <sup>75%</sup>	$P_{KS}$	Aver. $\pm\sigma$	Med. <sub>25%</sub> <sup>75%</sup>	$P_{KS}$	Aver. $\pm\sigma$	Med. <sub>25%</sub> <sup>75%</sup>	$P_{KS}$
RQ	202	0.13 $\pm$ 0.12	0.089 <sub>0.045</sub> <sup>0.167</sup>	10 <sup>-16</sup>	15.5 $\pm$ 1.1	15.5 <sub>14.7</sub> <sup>16.2</sup>	1.5 10 <sup>-4</sup>	-23.0 $\pm$ 1.8	-23.0 <sub>-24.1</sub> <sup>-21.6</sup>	10 <sup>-14</sup>
RL	76	0.35 $\pm$ 0.21	0.334 <sub>0.200</sub> <sup>0.530</sup>		16.1 $\pm$ 0.9	16.1 <sub>15.6</sub> <sup>16.5</sup>		-24.8 $\pm$ 1.8	-25.3 <sub>-26.2</sub> <sup>-24.2</sup>	

	M			L/M		
	Aver. $\pm\sigma$	Med. <sub>25%</sub> <sup>75%</sup>	$P_{KS}$	Aver. $\pm\sigma$	Med. <sub>25%</sub> <sup>75%</sup>	$P_{KS}$
RQ	8.21 $\pm$ 0.76	8.21 <sub>7.65</sub> <sup>8.79</sup>	10 <sup>-16</sup>	3.89 $\pm$ 0.53	3.95 <sub>3.49</sub> <sup>4.24</sup>	0.0017
RL	9.23 $\pm$ 0.60	9.24 <sub>8.92</sub> <sup>9.67</sup>		3.65 $\pm$ 0.47	3.63 <sub>3.37</sub> <sup>4.03</sup>	



**Figure 2.** Distribution of apparent V magnitude (left panels) and redshift  $z$  (right panels) for our 278 AGN sample. Shaded: RL; Unshaded: RQ. The left panel shows that, in our sample, RL sources are on average less bright than RQ sources while the right panel suggests a distribution favoring higher  $z$  for RL AGN.

distribution of the computed parameters M and L/M are also significantly different for RQ and RL samples.

RL sources are somewhat over-represented in the M03 sample, but not in the M03+G99 sample. Any over-representation can be properly quantified if we compare general population expectation for the number ratio between the number of RL sources and the total number of sources ( $f_R = N(RL)/[N(RL)+N(RQ)]$ ) in the  $M_B$  range covered by our sample. Weighting the luminosity-dependent  $f_R$  value from La Franca et al. (1994) over the  $M_B$  distribution of our sample (see Fig. 2 of M03) i.e., within  $-27 < M_B < -23$ , we obtain  $f_R \approx 25\%$  versus  $f_R \approx 39\%$  in M03 and  $f_R \approx 26\%$  in M03+G99.

More cumbersome are the biases shown in Fig. 2: RL sources tend to be fainter and more distant than RQ ones, as well as intrinsically more luminous. Biases that are affecting RL sources are not clear. RL core-dominated sources are over-represented in M03. This will contribute to bias the RL sample to higher L and  $z$  values (see Sulentic et al. 2003 for a more thorough discussion).

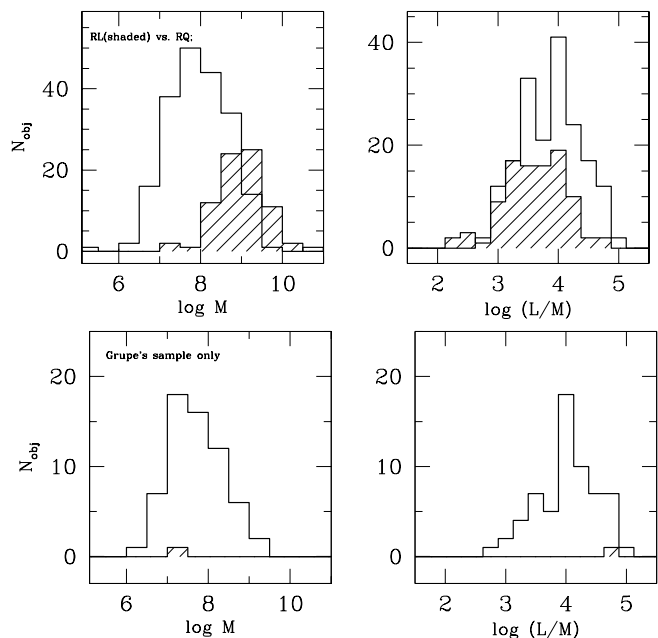


**Figure 3.** Distribution of M (left panels) and L/M ratio (right panels) for our sample (upper panels) and for the sample by Grupe et al. 1999 only. Shaded: RL; Unshaded: RQ. The left panel shows that RL sources shows larger M than RQ while the right panel suggests a largely overlapping L/M range for RQ and RL AGN, even if the largest L/M sources are almost all RQ.

### 5.1 Bootstrap Simulations

Are differences in redshift and luminosity distributions the cause of the inferred M and L/M differences between RQ and RL sources? We can use most of our sources in creating better matched subsamples out of our M03+G99 sample (bootstrap techniques, i.e. Efron & Tibshirani, 1993). The most important parameter appears to be redshift (which implies a strong bound on the apparent magnitude). We constructed pseudo-samples of RQ and RL sources *with similar redshift and apparent magnitude distributions*. More precisely: (1)

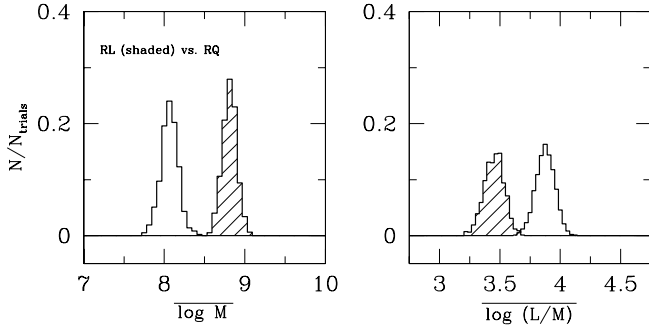


**Figure 4.** Results of bootstrap simulations. Distributions of average  $M$  (left) and  $L/M$  (right) for 1000 pseudo samples of 40 RL (shaded) and RQ objects with matching apparent magnitude and redshift distribution. Bootstrap simulations suggest that there are systematic differences in the sense that RL sources have large  $M$  and lower  $L/M$  ratios than RQ AGN.

we randomly selected two pseudo-samples with the same  $z$  and  $m_V$  distributions, indistinguishable within a  $2\sigma$  confidence limit, (2) we computed average  $\log M$  and  $\log L/M$  values for each pseudo-sample, (3) we repeated the selection  $\sim 1000$  times, (4) we computed the distribution of average  $\log M$  and  $\log L/M$  values for the pseudo-samples (the *bootstrapped* samples), (5) we derived the expectation values for  $\langle \log M \rangle$  and  $\langle \log L/M \rangle$  as the medians of the distributions for the bootstrapped samples, (6) we estimated the significance level of any difference from the average values and the dispersion of the distributions. While cannot eliminate biases from our sample, we can try to apply the same bias to both populations.

## 5.2 Matching $z$ and $m_V$ Distributions

The bootstrap procedure makes both the  $M$  and  $L/M$  differences stronger (see the upper panels of Fig.3 and Fig.4): the median values are  $\langle \log M(\text{RQ}) \rangle \approx 8.07 \pm 0.07$  vs.  $\langle \log M(\text{RL}) \rangle \approx 8.81 \pm 0.06$ , and  $\langle \log L/M(\text{RQ}) \rangle \approx 3.88 \pm 0.05$  vs.  $\langle \log L/M(\text{RL}) \rangle \approx 3.45 \pm 0.06$ . The results can be seen in Fig.3 (the original sample) and Fig.4 (after bootstrap simulations). Since matching  $m_V$  and  $z$  is equivalent to a match in  $L$ , it follows that the two plots are not independent, and that systematically larger  $\text{FWHM}(H\beta_{\text{BC}})$  drives a larger mass estimate for RL sources.

## 5.3 Same $z$ and $m_V$ Distribution with a Narrow Mass Range

To avoid sample biases, and to assess the reality of any  $L/M$  systematic difference, we restricted our attention to sources within a narrow mass range. At the same time, we retained the above conditions on the  $z$  and  $m_V$  distribution. The mass range was chosen so that we had the maximum possible number of sources:  $8.5 \lesssim \log M \lesssim 9.5$  with 48 sources (Fig. 5). No systematic difference in  $\log L/M$  ( $\lesssim 0.2$ ) is found. In a comparison of RQ and RL sources with the additional condition  $\text{FWHM}(H\beta_{\text{BC}}) \gtrsim 4000 \text{ km s}^{-1}$ , and matching the  $z$  and  $m_V$  distributions, we find again no systematic difference in either  $M$  or  $L/M$  distributions (see Fig. 6; note that the difference can be statistically significant, but it is

of the order of uncertainty in  $M$  and  $L/M$  determination and therefore too small to be of relevance). The similarity of the parameter space occupation for RQ and RL sources with  $\text{FWHM}(H\beta_{\text{BC}}) \gtrsim 4000 \text{ km s}^{-1}$  carries into a similarity in derived  $L/M$  and  $M$ . In other words, there is a large RQ population whose  $M$  and  $L/M$  values are similar to the ones of RL sources.

## 5.4 Population A and B: Understanding Biases

Sulentic et al. (2000a) introduced the concept of Population A [ $\text{FWHM}(H\beta_{\text{BC}}) \lesssim 4000 \text{ km s}^{-1}$ ] and Population B [ $\text{FWHM}(H\beta_{\text{BC}}) \gtrsim 4000 \text{ km s}^{-1}$ ] as fundamentally related to the BLR structural properties (Sulentic et al. 2000a,b). RQ sources dominate Pop. A (88 % of the total) and are about  $\frac{1}{2}$  of Pop. B sources. Most RL sources ( $\approx 75\%$ ) are Population B. Thus to a large extent a RL vs. RQ comparison is a Pop. A RQ vs. Pop. B RL comparison (as it was in the early study on CIV $\lambda 1549$  by Marziani et al. 1996).

The validity of the previous results on  $M$  and  $L/M$  difference depends on (1) the fraction of Pop. A RQ sources at low  $z$ , and on (2) whether most RL sources at  $z < 1$  are Pop. B. A proper assessment of the Pop. A/Pop. B ratio for RQ samples would imply a thorough analysis of the discovery biases affecting major surveys (see e.g., Oshlak et al. 2002). This goes far beyond the aim of the present paper.

Actually, we know that we have a bias favoring Pop. A RQ sources in the G99 sample. If we apply the same bootstrap analysis to the M03 sample only, we obtain a lower fraction of Pop. A sources ( $\approx 45\%$ ), but we reach the same qualitative conclusions. Therefore a significant bias may arise only if we *miss* a large fraction of Pop. B RQ sources ( $>20\%$ ). This does not seem the case. An analysis of the SDSS shows that NLSy1s should be  $\approx 15\%$  of all low- $z$  AGN (Williams et al. 2002). The ratio between NLSy1s and the rest of Pop. A (i.e., sources satisfying the criterion  $2000 \text{ km s}^{-1} \lesssim \text{FWHM}(H\beta_{\text{BC}}) \lesssim 4000 \text{ km s}^{-1}$ ) is  $\approx \frac{1}{3}$  (estimated on the whole M03 sample, on a restriction to PG sources). This implies that Pop. A should be  $\approx 60\%$  of all low  $z$  AGN. We note that: (a) in M03+G99, Pop. A sources account for  $\approx 52\%$  of all sources; (b) the ratio of NLSy1s to all RQ sources is  $\approx 15\text{--}20\%$  if we consider the M03 and M03+G99 independently, in line with the SDSS findings. Therefore, if there is a sample bias favoring one of the two populations, it is not strong.

Regarding the second issue, it has been possible to show that Fanaroff-Riley II quasars belong exclusively to Pop. B. RL sources with narrower lines [RL with  $\text{FWHM}(H\beta_{\text{BC}}) \lesssim 4000 \text{ km s}^{-1}$ ] are predominantly core-dominated (CD) sources, and therefore likely to be a less frequent, beamed population of preferentially aligned sources in a FR II/CD unification scenario (Sulentic et al. 2003).

Even if the amplitude of the  $L/M$  and  $M$  systematic difference will of course depend on sample definition, such difference is unlikely to be caused by selection effects, and should be considered real. This is in line with recent research pointing toward systematic differences in the mass function of RQ and RL AGN (as discussed in §8.2).

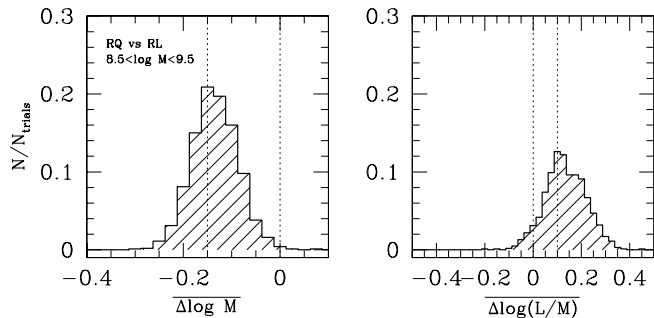


**Figure 5.** Distribution of  $\Delta \overline{\log M} = \overline{\log M(RQ)} - \overline{\log M(RL)}$  (left panel) and  $\Delta \overline{\log L/M} = \overline{\log L/M(RQ)} - \overline{\log L/M(RL)}$  (right panel) for  $\sim 1000$  pseudo samples of RL and RQ sources.  $m_V$  and  $z$  distributions were matched, and a restriction to the  $M$  was applied:  $8.5 \leq \log M \leq 9.5$  (48 sources). RL and RQ quasars have almost the same  $L/M$  ratio distributions.

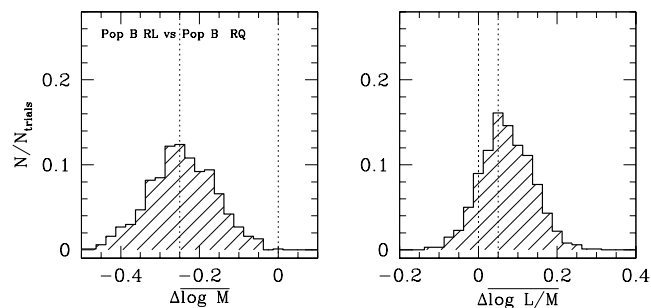


**Figure 6.** Distribution of  $\Delta \overline{\log M}$  (left panels) and  $\Delta \overline{\log L/M}$  (right panels) for  $\sim 1000$  pseudo samples of 40 objects with  $\text{FWHM}(H\beta_{BC}) \geq 4000 \text{ km s}^{-1}$  but separated on the basis of radio loudness. It points that RL and RQ Pop. B are not distinguishable on the basis of  $M$  or  $L/M$ .

## 6 $H\beta_{BC}$ PROFILE SHAPE

### 6.1 The Influence of $M$ and $L/M$

We generated median  $H\beta_{BC}$  profiles in bins covering narrow ranges of derived  $M$  and  $L/M$ . The adopted binning is shown in Fig. 7. The median spectra (normalized to the local continuum) are plotted in Fig. 8. Table 2 provides, for every bin, average measures of the  $H\beta_{BC}$  profile centroid at 1/4 and 1/2 peak intensity, the best fit to the profile shape, and the intensity ratio ( $C2/C1$ ) in case when two components have been used.

The median  $H\beta_{BC}$  profile computed for each bin (see Fig. 9 and 10) suggests that:

- a Lorentz function provides good fits to median profiles in bins for which  $3.9 < \log L/M < 4.4$ , and for  $3.4 < \log L/M < 3.9$  and  $7.5 < \log M < 8.5$ . Profile models employing Gaussian functions yield poorer fits with significantly larger  $\chi^2$ . The slight redward asymmetry in the bin  $3.9 < \log L/M < 4.4$  and  $8.5 < \log L/M < 9.5$  can be modeled by adding a weak, redshifted Gaussian component  $C2$  with  $C2/C1 \approx 0.1$ . Similar considerations apply to the bin

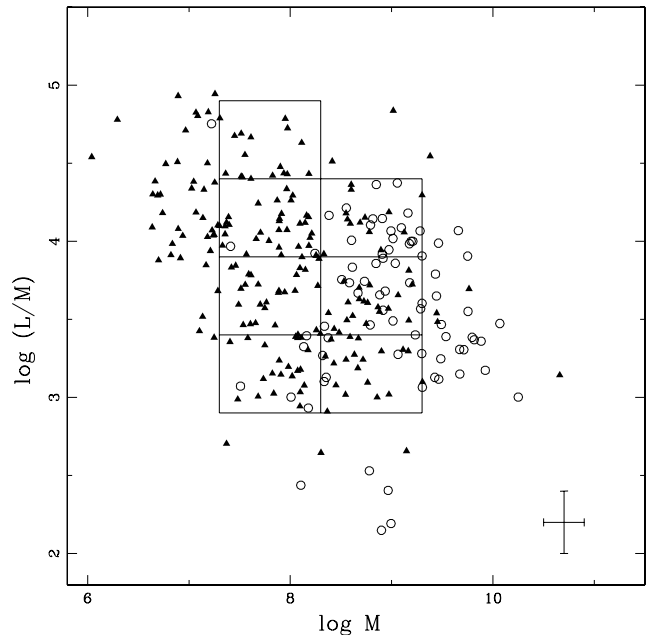


**Figure 7.** Binning of our sample in the  $L/M$  vs.  $M$  parameter space for the median spectra computations. Symbols are as in Figure 1.

$4.4 < \log L/M < 4.9$  and  $7.5 < \log M < 8.5$  (i.e., largest  $L/M$ , possibly super-Eddington, and lowest  $M$ ) profile: a slight blueward asymmetry visible in the median profile can be modeled as an additional, blueshifted component contributing  $\sim 0.1$  of the total line emission.

- If  $\log L/M < 3.4$ , profiles are better fit with double Gaussian models than using a Lorentz core + broader Gaussian component. The latter model is favored if the narrow component of  $H\beta$  is *not* subtracted (e.g. Oshlack et al. 2002, but lack of narrow component subtraction will also lead to an underestimate of  $M$ ).

- The “red shelf” or redshifted Gaussian component (we refer to it as very broad line region (VBLR) component) appears to be strongly influenced by  $M$ , i.e. larger  $M$  sources show a more prominent VBLR component, as well as by  $L/M$  (this is especially evident from the values for  $8.5 < \log M \leq 9.5$  reported in Table 2). The  $M$  dependence is easily seen by comparing the solid (lower mass) and overlaid dashed (higher mass) profiles in each frame of Figure 8. Table 3 shows that  $c(1/4)$  measures are significantly redshifted for the bins corresponding to larger  $M$ .

Best fits to  $H\beta_{BC}$  and individual line components are shown in Fig. 9. Fig. 10 illustrates a case in which the exchange from a Lorentzian to a Gaussian significantly worsen residuals. The case shown is the one where fits provides more similar results. In general exchanging functional forms from the best fitting ones imply larger differences and a  $\chi^2$  worsening by a factor of  $\approx 2$ .

### 6.2 Influence of Radio Loudness on $H\beta_{BC}$

Is the  $H\beta_{BC}$  profile shape influenced by radio loudness? To answer this question we generated the  $H\beta_{BC}$  profile (see Fig. 11) for the interval  $8.5 < \log M < 9.5$  and *any*  $L/M$

**Table 2.**  $H\beta_{BC}$  line centroids at 1/4 and 1/2 fractional intensity as a function of  $\log L/M$ . For each interval of  $\log L/M$  the table reports the  $H\beta_{BC}$  best fitting function (FF; either Lorentzian (L) or Gaussian (G)), and their peak position and FWHM. In case two component are needed for the best fit, their intensity ratio (C2/C1) is reported in the last column.

log L/M	c(1/4)	c(1/2)	FWHM	Best Fit						
				1 <sup>st</sup> Component			2 <sup>nd</sup> Component			C2/C1
				FF	Peak	FWHM	FF	Peak	FWHM	
[km s <sup>-1</sup> ]	[km s <sup>-1</sup> ]	[km s <sup>-1</sup> ]		[km s <sup>-1</sup> ]	[km s <sup>-1</sup> ]		[km s <sup>-1</sup> ]	[km s <sup>-1</sup> ]		
7.5 ≤ logM ≤ 8.5										
4.4–4.9	-170 <sup>+290</sup> <sub>-390</sub>	-55 <sup>+120</sup> <sub>-110</sub>	1410±110	L	50	1400	G	-1850	2100	0.09
3.9–4.4	+140 <sup>+400</sup> <sub>-390</sub>	+80 <sup>+160</sup> <sub>-160</sub>	2310±160	L	-5	2350	...	...	...	...
3.5–3.9	+140 <sup>+500</sup> <sub>-540</sub>	+200 <sup>+240</sup> <sub>-240</sub>	3200±240	L	50	3500	...	...	...	...
2.9–3.4	+400 <sup>+780</sup> <sub>-600</sub>	-85 <sup>+310</sup> <sub>-310</sub>	5490±310	G	-320	4000	G	+1400	10000	0.73
8.5 < logM ≤ 9.5										
3.9–4.4	+330 <sup>+620</sup> <sub>-560</sub>	+250 <sup>+250</sup> <sub>-240</sub>	3100±250	L	+1	3000	G	+4000	7600	0.12
3.5–3.9	+915 <sup>+1100</sup> <sub>-790</sub>	+440 <sup>+320</sup> <sub>-320</sub>	4900±320	G	-20	2900	G	+1050	8700	1.7
2.9–3.4	+2320 <sup>+1060</sup> <sub>-1090</sub>	+314 <sup>+400</sup> <sub>-380</sub>	7000±400	G	-70	4900	G	+2100	12600	1.09

for RQ and RL separately ( $N_{RQ} = 56$ ,  $N_{RL} = 36$ ). Fig. 11 shows that the composite spectra of RL and RQ objects are different: the narrow lines ( $[OIII]\lambda\lambda 4959, 5007$  and  $H\beta_{NC}$ ) are stronger and  $W(H\beta_{BC})$  is lower in RL objects. At the same time, the  $H\beta_{BC}$  profiles remain indistinguishable within our S/N limits (see Fig. 11). To further check this result we additionally generated the composite spectra separating RL and RQ objects in three other M and L/M ranges: (a)  $8.5 < \log M < 9.5$  and  $3.9 < \log L/M < 4.4$  ( $N_{RQ} = 14$ ,  $N_{RL} = 19$ ); (b)  $8.5 < \log M < 9.5$  and  $3.4 < \log L/M < 3.9$  ( $N_{RQ} = 26$ ,  $N_{RL} = 13$ ); (c) and  $8.0 < \log M < 9.0$  and  $3.9 < \log L/M < 4.4$  ( $N_{RQ} = 14$ ,  $N_{RL} = 19$ ). Although the S/N ratio of the composites was lower since fewer objects were used, results were similar: indistinguishable  $H\beta_{BC}$  profiles and centroids, with higher  $W([OIII]\lambda\lambda 4959, 5007)$  and lower  $W(H\beta_{BC})$  for RL objects. We conclude that the  $H\beta_{BC}$  line profile shape does not depend strongly on radio loudness.

## 7 THE “BLUE OUTLIERS”

### 7.1 Spectral Properties of $[OIII]\lambda\lambda 4959, 5007$ “Blue Outliers”

In a previous investigation (Zamanov et al. 2002), we identified seven objects from the M03 sample that showed an  $[OIII]\lambda\lambda 4959, 5007$  blueshift relative to the peak of  $H\beta$ . The shift amplitudes were  $\geq 250$  km s<sup>-1</sup> leaving little doubt that we are observing a significant velocity displacement. We have identified five additional AGN that show large amplitude blueshifts among the objects of G99. Some properties of all of these sources are given in Table 3. All of the sources show strong Fe II<sub>opt</sub> emission. In the E1 context they show: (1)  $R_{FeII} \gtrsim 0.5$ , (2)  $FWHM(H\beta) < 4000$  km s<sup>-1</sup> (i.e., they are located in spectral bins A2 and A3 of Sulentic et al. 2002); (3) a large C IV  $\lambda 1549$  broad component blueshift (Zamanov et al. 2002). Blue outliers show also weak  $[OIII]\lambda\lambda 4959, 5007$  emission with  $W([OIII]\lambda 5007) \lesssim 20$  Å, and a median value of  $\approx 6$  Å.

Nine out of our 12 outliers are formally NLSy1s. In general, the  $[OIII]\lambda\lambda 4959, 5007$  lines of NLSy1s have a relatively narrow profile with often, in addition, a second broader, blueshifted component (Véron-Cetty, Véron & Gonçalves 2001). The blue-shift, is  $400 - 1100$  km s<sup>-1</sup> when the two components can be deblended (Zheng et al. 2002). These values correspond to the blue outliers range suggesting that the latter are an extreme subset with low  $W([OIII]\lambda 5007)$  when only the shifted component is visible.

### 7.2 FWHM of Fe II<sub>opt</sub> and $[OIII]\lambda\lambda 4959, 5007$ lines

Computation of M requires that  $H\beta_{BC}$  be separated from any narrow component so that  $FWHM(H\beta_{BC})$  can be properly measured. The problem is that extreme sources like the blue outliers show no profile inflection (reflected in the fact that they are well fit by a Lorentzian function). The rationale for our methodology has been detailed in M03, and will not be rediscussed here. We just remind that we normally assume (and find) that the narrow component of  $H\beta$  shows almost the same shift and width properties as the  $[OIII]\lambda\lambda 4959, 5007$  lines. However, in blue outliers  $W([OIII]\lambda 5007)$  is smaller than in any broad emission line AGN class and is also blueshifted relative to the peak of  $H\beta$ . We conclude that we are not measuring a narrow line component at the Lorentzian tip of the  $H\beta$  profile. Any narrow component of  $H\beta$  is assumed to be blueshifted and lost in the blue wing of the broad line (even assuming it has the same strength as  $[OIII]\lambda 5007$  in blue outliers it would represent less than 10% of the total line flux). Subtraction of a narrow  $H\beta$  component would have a non-negligible effect on the  $FWHM(H\beta_{BC})$  measurement which is needed for the M estimation.

The Fe II  $\lambda 4570$  feature is a complex of lines thought to have FWHM similar to  $H\beta_{BC}$ . We estimated  $FWHM(Fe II \lambda 4570)$  *independently* from  $FWHM(H\beta_{BC})$  by Fe II<sub>opt</sub> template fitting using the I Zw 1 spectrum (of course, only for highest S/N spectra; see M03 for

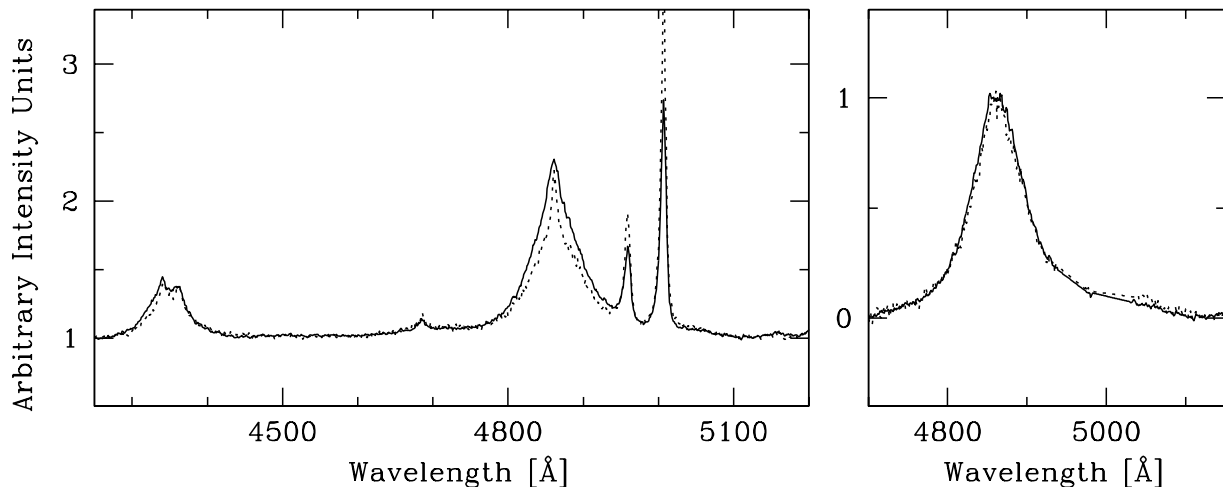


**Figure 11.** Comparison of the RQ and RL objects in the mass interval  $8.5 < \log M < 9.5$  and any L/M ratio ( $N_{RQ} = 56$ ,  $N_{RL} = 36$ ). **(left)** Comparison of the composite spectra of RQ and RL (after subtraction of the Fe II<sub>opt</sub> template).  $W(H\beta_{BC})$  is 20% higher in RQ,  $W([OIII]\lambda 5007)$  is 35% higher in RL. **(right)** cleaned and scaled  $H\beta_{BC}$  profile. The  $H\beta_{BC}$  profiles of RQ and RL are almost identical.

details). In our sample  $FWHM(FeII\lambda 4570)$  is similar to  $FWHM(H\beta_{BC})$  with few exceptions only (see Bongardo et al. 2002). Estimated  $FWHM(FeII\lambda 4570)$  values are given in Table 3. No narrow FeII $\lambda 4570$  component has been detected and nor is one expected given the low inferred density for the narrow line region. In principle, we can use  $FWHM(FeII\lambda 4570)$  instead of  $FWHM(H\beta_{BC})$  in the mass derivations in order to avoid any error associated with a narrow line component. Use of  $FWHM(FeII\lambda 4570)$  instead of  $FWHM(H\beta_{BC})$  will yield M values within  $\sim 10\%$  of ones derived from  $FWHM(H\beta_{BC})$ .

The correlation of nuclear BH mass with stellar bulge velocity dispersion  $\sigma_*$  is now well established in nearby galaxies. Recent results (Nelson 2000; Boroson 2002) show that a BH mass –  $FWHM([OIII]\lambda 5007)$  correlation is also present but with larger scatter. The  $FWHM([OIII]\lambda 5007)$  measures given in Table 3 provide another way to estimate BH masses. The derived values are however considerably higher than values calculated using  $FWHM(H\beta_{BC})$  and source luminosity. This is not surprising because NLSy1-type AGN apparently do not follow Nelson’s relation (Mathur, Kuraszkiwicz & Czerny 2001). If NLSy1s do not follow the relation then blue outliers will almost certainly show the same lack of agreement. This does not contradict our assumption that blueshifted  $[OIII]\lambda\lambda 4959, 5007$  arises in outflowing gas (Zamanov et al. 2002), possibly associated with a disk wind. The  $[OIII]\lambda\lambda 4959, 5007$  region in blue outliers may be very compact and its velocity field is not likely to be dynamically related to the host galaxy stellar bulge. This points to a limiting  $W([OIII]\lambda 5007)$  ( $\approx 20\text{\AA}$ ) below which  $FWHM([OIII]\lambda\lambda 4959, 5007)$  emission ceases to be a useful mass estimator.

### 7.3 $M_B$ and L/M Ratio of [OIII] Outliers

All blue outliers lie in the region of E1 thought to be populated by highly accreting (high L/M) sources (Marziani et al. 2001). Most of them are located close to the Edding-

ton limit ( $\log L/M \approx 4.53$ , see Fig.12). This is also true if: (1)  $FWHM(FeII\lambda 4570)$  is used instead of  $FWHM(H\beta_{BC})$  to derive M, and (2) an orientation correction is applied. The blue outliers may be oriented close to pole-on. Since  $M \propto FWHM^2$ , an inclination correction will move the “blue outliers” toward higher mass and lower L/M (see the arrows on Fig.12). Even with an inclination correction by a factor  $\approx 4$ , the L/M values for blue outliers remain among the highest observed. We note that: (1) other sources should also be corrected for orientation especially if low ionization lines are emitted in a flattened configuration in all Population A sources, as suggested (Marziani et al. 1996); (2) some care is needed since we neglected a photometric correction which is basically unknown. We do not know whether any sort of continuum beaming operates for RQ AGN as  $i \rightarrow 0^\circ$  (very similar  $W(H\beta_{BC})$  for CD and LD RL sources suggests no strong effect; Sulentic et al. 2003). Observational errors and uncertainty in the orientation correction do not allow us to determine whether some blue outliers are really super-Eddington sources as they appear in Fig.12.

All blue outliers show estimated masses less than  $10^{8.5} M_\odot$ . We tried to determine if the blue outliers large L/M was a consequence of a low-mass bias by calculating the  $M_B$  difference between blue outliers and other sources in two mass ranges: (1)  $7.15 \leq \log M \leq 8.45$  (where the “blue outliers” are before the orientation correction) and (2)  $7.55 \leq \log M \leq 8.85$  (where they move after the orientation correction). Table 4 shows that the blue outliers are almost certainly  $\sim 1$  mag brighter than other sources with similar mass implying 2–3 times higher L/M ratios.

## 8 DISCUSSION

### 8.1 Mass-Luminosity Diagram

The ranges of M and L/M considered in this study are similar to those in other recent work (Woo & Urry 2002a; Collin et al. 2002). We find that the Eddington limit de-



**Table 3.** The spectral properties of the “blue outliers”: radial velocity difference between top of H $\beta$  and [OIII] $\lambda$ 5007, equivalent width and FWHM of [OIII] $\lambda$ 5007, FWHM of FeII $\lambda$ 4570, the equivalent widths ratio of FeII $\lambda$ 4570 and H $\beta$ <sub>BC</sub> ( $R_{\text{FeII}}$ ).

Name	$\Delta v$ [km s <sup>-1</sup> ]	W[OIII] $\lambda$ 5007 [ Å ]	FWHM[OIII] [km s <sup>-1</sup> ]	FWHM(H $\beta$ ) [km s <sup>-1</sup> ]	FWHM(FeII) [km s <sup>-1</sup> ]	RFe
I Zw 1	-640	15.3	1440 $\pm$ 120	1092	1095	1.30 $\pm$ 0.1
PKS 0736+01*	-430	2.6	720 $\pm$ 60	3258	3560	0.70 $\pm$ 0.1
PG 0804+761	-305	10.1	780 $\pm$ 60	3302	3067	0.42 $\pm$ 0.1
PG 1001+291	-680	3.4	960 $\pm$ 60	1759	1588	0.71 $\pm$ 0.1
PG 1402+261	-300	2.6	900 $\pm$ 180	1938	1957	0.73 $\pm$ 0.1
PG 1415+451	-600	2.9	660 $\pm$ 60	2555	2870	0.66 $\pm$ 0.1
PG 1543+489	-950	6.5	—	1555	1588	0.64 $\pm$ 0.1
RX J0136.9-3510	-380	6.0	900 $\pm$ 60	1050	1100	1.0 $\pm$ 0.1
RX J0439.7-4540	-580	5.0	1020 $\pm$ 120	1020	1100	0.9 $\pm$ 0.1
RX J2217.9-5941	-330	8.1	1140 $\pm$ 120	1370	1588	2.0 $\pm$ 0.2
RX J2340.6-5329	-490	21.8	780 $\pm$ 60	1228	1588	1.3 $\pm$ 0.1
MS 2340.9-1511	-420	5.8	780 $\pm$ 60	969	1218	1.1 $\pm$ 0.1

\* RL CD source

**Table 4.**  $M_B$  of the “blue outliers” (as they are given in Véron-Cetty & Véron catalog without correction for the cosmology), compared with other objects in the sample with similar mass.  $P_{\text{KS}}$  is the probability that the “blue outliers” and the other objects in the indicated mass ranges are randomly drawn from the same parent population according to Kolmogorov-Smirnov test.

	Aver. $\pm\sigma$	Med. <sup>75%</sup> <sub>25%</sub>	$P_{\text{KS}}$
blue outliers	-23.9 $\pm$ 0.8	-23.85 <sup>-23.45</sup> <sub>-24.30</sub>	
7.0 $\leq$ logM $\leq$ 8.2	-22.4 $\pm$ 0.8	-22.20 <sup>-21.50</sup> <sub>-23.40</sub>	0.00035
7.6 $\leq$ logM $\leq$ 8.8	-22.8 $\pm$ 0.8	-22.90 <sup>-21.80</sup> <sub>-23.90</sub>	0.00600

defines an approximate upper boundary to the luminosity distribution (as in Woo & Urry 2002a), indicating that there are no known low- $z$  AGN accreting significantly above the Eddington limit (this depends on the adopted  $H_0$  value). Figure 1 also suggests that there may be fewer high (than low) mass sources with L/M close to the Eddington limit. This might be a selection effect or an indication that galaxies with a high mass BH may be unable to supply fuel at high L/M. In other words, the upper envelope in Figure 1 might be due to the Eddington limit as well as the ability of the surrounding matter to feed the accretion flow (see, e.g., Nicastro et al. 2003). The lower envelope of the luminosity distribution may be due to a selection effect (e.g. Woo & Urry 2002a), or it may indicate that only sources radiating at  $0.01 \lesssim (L/L_{\text{Edd}}) \lesssim 1.00$  exhibit a stable broad lines region. The latter possibility might be connected with the presence/absence of an accretion disk wind (see also Kollatschny & Bischoff 2002).

## 8.2 On the Difference Between Radio Loud and Radio Quiet AGN

Somewhat confusing claims have been recently made on the difference between RL and RQ sources in terms of M and L/M. Laor (2000) found that the radio loudness is strongly related to M. Woo & Urry (2002b) concluded that radio loudness does not depend strongly on M. Lacy et al. (2001)

found no evidences for critical M or L/M ratio that turns on powerful radio jets. Ho (2002) showed that the dependence of radio loudness on M disappears altogether when one considers AGN with a broad range of intrinsic luminosity. At the same time he found that radio loudness seems to be related to the mass accretion rate. RL and RQ sources are well separated *in terms of* M by the new Eigenvector analysis of Boroson (2002).

The difference between RQ and RL on Eigenvectors diagram (Boroson 2002) is probably connected with the inclusion of [OIII] $\lambda$ 5007 line parameters. In RL quasars part of the [OIII] $\lambda$ 4959,5007 is coming from extended regions connected with the radio jet (Wilman, Johnstone & Crawford 2000). Previous work has shown that RL activity in low M sources may be physically possible. Our sample contains a RL NLSy1 that is one of the highest L/M sources, and other sources that radiate at  $\log L/M \approx 4.5$ . Our analysis stressed that there are no appreciable effects (within the limits set by our S/N) on the H $\beta$ <sub>BC</sub> profile attributable to radio loudness, and that *Pop. B* RL and RQ sources can have the same M and L/M values. Therefore, *it is not unreasonable to conclude that a similar range of M and L/M is physically possible for both RQ and RL sources.* However, this does not mean that the mass function for RL and RQ sources is necessarily the same. A robust inference from the bootstrap analysis reported in §5.1 is that the mass function and the conditional probability of having certain L/M values at fixed M are likely to be different for the two AGN classes. A correct estimation of the mass function and of the L/M probability distribution demands a more thorough analysis that includes selection biases. In addition, the RL/RQ dichotomy is probably related to parameters other than M and L/M, such as BH spin and morphological segregation. We suggest that the intrinsic mass function and L/M distribution differences as well as jet-related effects like [OIII] $\lambda$ 4959,5007 enhancement in RL sources and sample selection criteria may drive the RQ/RL separation shown by Laor (2000) and Boroson (2002).

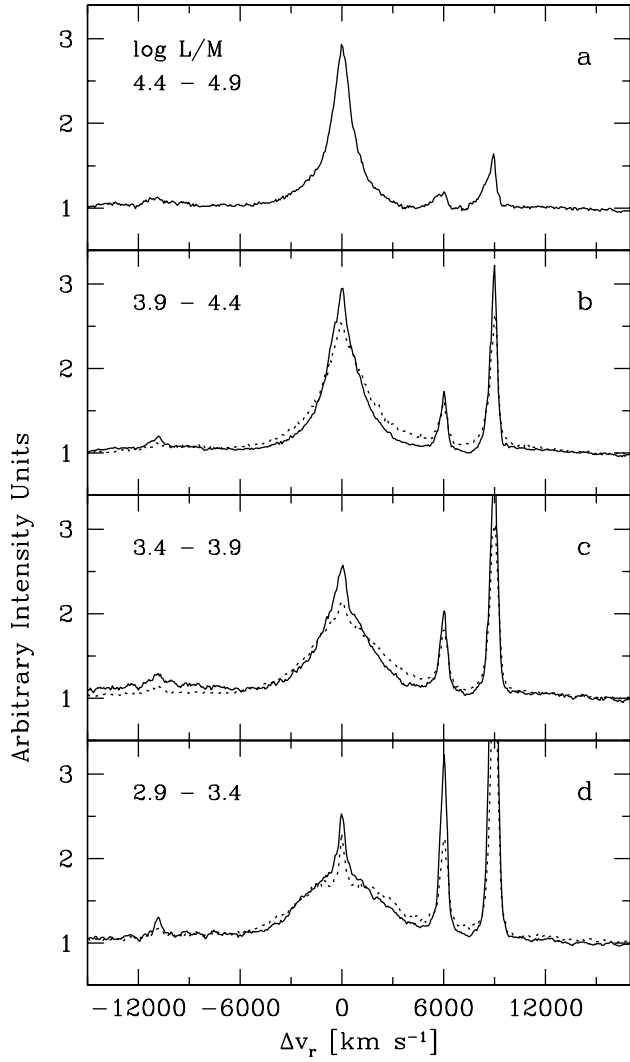


**Figure 8.**  $H\beta$  line profiles after  $\text{FeII}_{\text{opt}}$  subtraction. From top to bottom the plots correspond to: (a)  $\log L/M$  4.4 - 4.9; (b)  $\log L/M$  3.9 - 4.4; (c)  $\log L/M$  3.4 - 3.9; (d)  $\log L/M$  2.9 - 3.4. Note that  $\log L/M \approx 4.53$  corresponds to  $L/L_{\text{Edd}} \approx 1$ . Solid lines correspond to  $7.3 \leq \log M \leq 8.3$ , and dashed lines to  $8.3 < \log M \leq 9.3$ .

### 8.3 Transition in $H\beta_{\text{BC}}$ Line Profile Shape

Connecting empirical and physical parameters, we find that median profiles for  $H\beta_{\text{BC}}$  in Pop. A sources ( $\log L/M > 3.9$ , and for  $3.5 < \log L/M < 3.9$  and  $7.5 < \log L/M < 8.5$ ) show a Lorentzian shape. In other words, if  $\log L/M \gtrsim 3.9$ , the shape is Lorentzian for all values of  $M$ . Similarly, if  $\log L/M \lesssim 3.4$  (bins dominated by Pop. B sources), the profile is redward asymmetric and can be decomposed into two Gaussian components (one redshifted and the other not). This suggests that the transition from Lorentzian to double Gaussian profiles is governed by a critical  $L/M$  value (it is interesting to note that the  $H\beta_{\text{BC}}$  asymmetry is also one of the major correlate of the original E1 of Boroson & Green 1992). Unfortunately, the division of the bins in the  $L/M$  strip  $3.4 < \log L/M < 3.9$  did not make the situation clearer. We conclude that the Lorentzian - double Gaussian profile transition occurs between  $3.4 \lesssim \log L/M \lesssim 3.9$  ( $0.08 \lesssim$

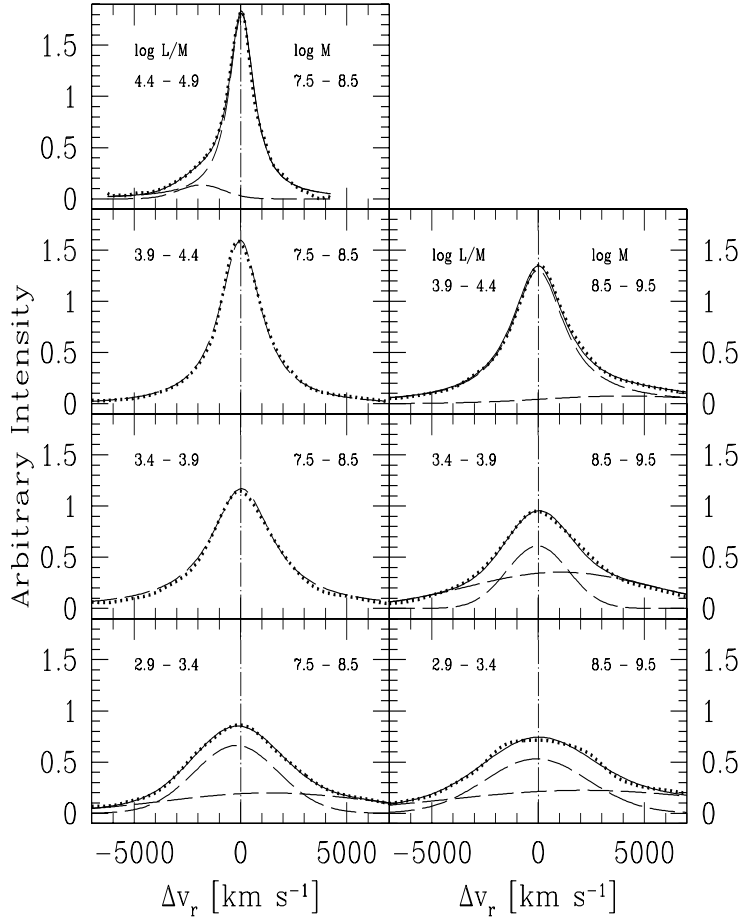


**Figure 9.**  $H\beta_{\text{BC}}$  line profile fitting after continuum,  $\text{FeII}_{\text{opt}}$  and  $H\beta_{\text{NC}}$  subtraction for the intervals in  $\log L/M$  and  $M$  defined in Table 2. The “cleaned”  $H\beta_{\text{BC}}$  (dotted line) is shown along with single fitting components (dashed lines) and with the resulting best fit (thin solid line).

$L/L_{\text{Edd}} \lesssim 0.25$ ). A more precise value would require knowledge of source orientation effects and a better-constrained  $\alpha$  value. This provides a physical basis for the phenomenological finding about profile change at  $\text{FWHM}(H\beta_{\text{BC}}) \approx 4000 \text{ km s}^{-1}$  and the resulting Population A-B hypothesis (Sulentic et al. 2002).

#### 8.3.1 $c(1/4)$ $H\beta_{\text{BC}}$ Dependence on Mass: Not Only Gravitational Redshift

We remark that a Double Gaussian fit to  $H\beta_{\text{BC}}$  in Pop. B sources is a formal result: two components are required to account for the redward asymmetry. The two components have a physical justification if, for example, the broader (VBLR) one can be ascribed to gas that lies closest to the continuum source in an optically thin (to the HI ionizing continuum) region with large covering factor  $f_c \approx 1$  (as defined in Sulentic & Marziani 1993 and Brotherton 1996). A new result from this investigation is that the amplitude of the redward asymmetry is mass dependent.

The  $c(1/4)$  dependence on  $M$  (for  $\Delta \log M \approx 1$  we ob-

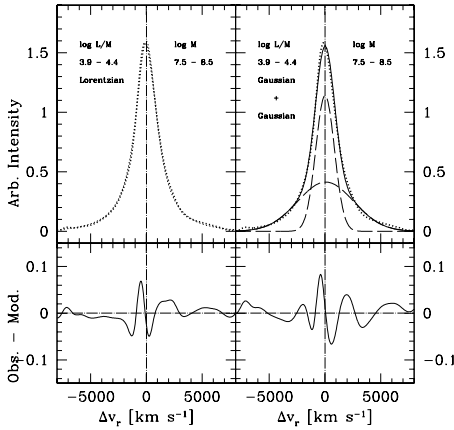


**Figure 10.** Example of  $H\beta_{BC}$  line profile fitting with different functional forms. The upper panes show the  $H\beta_{BC}$  (dotted lines) fit by a Lorentzian (left, best fit identical to Fig. 9) and to a double Gaussian. The lower panel show residuals for both cases. The Lorentzian fit is significantly better, yielding to a decrease in  $\chi^2$  by a factor  $\approx 1.5$ . This is the most doubtful case among the ones considered in this study; in all other cases a Lorentzian/Gaussian exchange from best fits yields a  $\chi^2$  worsening by a factor  $\approx 2$ .

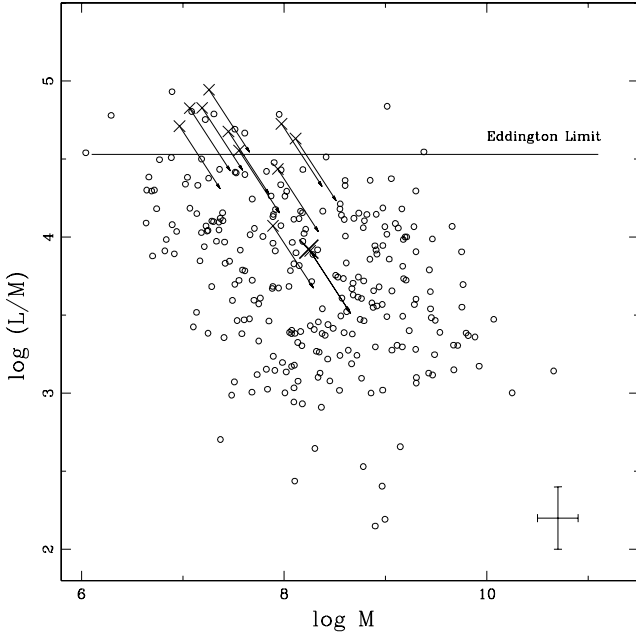


**Figure 12.** Position of blue outliers (crosses) relative to other sources in our sample (open circles). The larger cross indicates the position of PKS 0736+01 - the only known RL “blue outlier”. The dashed line indicates the Eddington limit. Arrows indicate displacements of blue outliers if we apply an orientation correction  $\sim 0.4$  to the derived masses. Blue outliers are among the highest  $L/M$  sources and remain in the upper part of the diagram even after an orientation correction. One should consider that many other sources would move in the same direction of the blue outliers if a proper orientation were applied to all sources.

tain a factor  $\approx 6$  increase in the  $c(1/4)$  redward displacement) means that we can try to ascribe the presence of the “red shelf”/VBLR component and the redward asymmetry to gravitational and transverse redshift (e. g., Corbin 1997). If the VBLR redshift is gravitational and transverse taking the  $c(1/4)$  value as a conservative estimate, we obtain the following distances from the central continuum source for the line emitting gas: if  $3.5 \lesssim \log L/M \lesssim 3.9$ ,  $r \approx 0.005$  pc and  $0.01$  pc for  $\log M = 8$  and  $\log M = 9$  respectively. In the case of the largest VBLR redshifts, the shift in radial velocity is  $\Delta v_r \approx 2300$  km s $^{-1}$  and we find  $r \approx 0.015$  pc  $\approx 170$  gravitational radii for  $\log M = 9$ . If we model the VBLR gas as a shell ( $f_c \approx 1$ ) with optical depth to the Lyman continuum  $\tau \lesssim 1$ , a CLOUDY (Ferland 2000) simulation shows luminosity of  $H\beta$   $\log L(H\beta)_{VBC} \approx 41.7$ , where the line luminosity is in ergs s $^{-1}$ . This falls far short in explaining the VBLR luminosity for sources in bin  $3.5 < \log L/M < 3.9$ ,  $8.5 < \log M < 9.5$ . The average  $\overline{\log L(H\beta)_{BC}}$  is 43.08. The VBLR contributes 2/3 of the total, so the VBLR average luminosity is  $\overline{\log L(H\beta)_{VBC}} \approx 42.9$ . The difference between the expected and observed VBLR luminosity is largely a consequence of the small shell radius required to explain the large  $\Delta v_r$  in the  $c(1/4)$ . In addition, the assumption of  $c(1/4)$  being dominated by gravitational + transverse redshift implies that  $z_{grav} \approx 3/2(FWHM/c)^2$ , which is not observed. We conclude that, even if  $c(1/4)$  is mass dependent, the  $c(1/4)$  shift amplitude cannot be explained by gravitational + transverse redshift alone. Once the stringent (and perhaps unphysical) distances from the central continuum sources set by gravitational redshift are relaxed, we note that our VBLR model can explain  $H\beta$  VBLR luminosity with reasonable shell radii. While this issue requires further investigation, it is tempting to suggest that we may be observing the long-sought infall, and that we are observing it easily because of the low optical depth expected also along the line of sight to  $H\beta$ . This would straightforwardly explain the ubiquitous presence of a strong  $H\beta_{BC}$  redward asymmetries at low  $L/M$ .

#### 8.4 On the Nature of the Blue Outliers

We observe “blue outliers” (following the simple wind model of Zamanov et al. 2002) when the [OIII] $\lambda\lambda 4959, 5007$  lines and the peak of  $H\beta$  arise in different regions -  $H\beta$  from a near face-on accretion disk and [OIII] from a wind with velocity of about 1000 km s $^{-1}$ . In terms of orientation these RQ sources would be analogous to some CD RL quasars or even to BL Lac (blazars). Other nearly-as-large  $L/M$  oriented sources can/must exist in our sample but they are not “blue outliers” for at least two reasons: (i) they possess a well developed Narrow Line Region (NLR) which is unlikely to show a significant blue-shifted component; (ii) they are not oriented face-on. There are probably also lower  $L/M$  sources oriented face-on, however their  $L/M$  ratio may not be sufficient to power a wind or the wind outflow velocity may be low (roughly  $< 300$  km s $^{-1}$ ). This could explain why the blue outliers are exclusively sources with very high  $L/M$ . It is worth noting that the only RL blue outlier, PKS 0736+01, is a flat spectrum radio source, and one of the brightest High Polarization, Optically Violently Variable sources. Its optical continuum is dominated by a “blazar” component as in BL Lac (Malkan & Moore 1986). Continuum proper-

ties suggest relativistic beaming making this a true pole-on RL source consistent with the interpretation of the “blue outliers” proposed by Zamanov et al. (2002).

In the most recent scenarios for joint AGN and galaxy evolution (e.g., Granato et al. 2001), the active nucleus and the galaxy evolve together, with BH accreting matter and the galaxy making stars and supplying fuel for the quasar. At some point, the wind from the accreting BH blows away the matter surrounding it and a quasar emerges. The central accretion source then appears as an unobscured quasar which lasts as long as there is fuel in the accretion disk (Fabian 1999). In this scenario our “blue outliers” could represent the stage when the quasar has just emerged (cf. Krongold et al. 2001 for a similar interpretation stemming from the analysis of NLSy1 host galaxies and environment). They could be in process of building of their NLR.

## 9 CONCLUSIONS

In this paper we computed virial masses and Eddington ratios for a sample of  $\sim 300$  AGN. We have shown that  $L/M$  seems to govern the overall shape of the  $H\beta_{BC}$ , and we found an interesting dependence on  $M$  of the  $H\beta_{BC}$  asymmetry. The transition between sources showing Lorentzian and double Gaussian  $H\beta_{BC}$  profiles is likely associated with a critical  $L/M$  value, as suggested by Sulentic et al. (2002).  $L/M$  and  $M$  values in the range  $8 \lesssim M \lesssim 9.5$  and  $3 \lesssim \log L/M \lesssim 4.2$  are found likely for both RL and RQ AGN while others ( $\log L/M \gtrsim 4.2$ ) may very unlikely for RL sources. However, it is important to stress the existence of a radio-loud blue outlier radiating at very high  $L/M$  ( $\log L/M \approx 4.8$ ; other RL sources radiate at  $\log L/M \approx 4.4$ ). This shows that there is no physical impossibility for RL sources to be of large  $L/M$  and small  $M$ ; they may be simply less likely to be that way.

We confirm that the “blue outliers” are mainly NLSy1 sources (Zamanov et al. 2002; see also Sulentic et al. 2000a). We increase the number of known “blue outliers” to 12. We show that all blue outliers are accreting at 2 times higher Eddington ratio than other sources with similar mass. The compactness of their NLR points toward very young ages (Zamanov et al. 2002), suggesting that they may be “fledgling” AGN as discussed for NLSy1 by Sulentic et al. (2000a) and Mathur (2000). An interesting issue is then whether different  $M$  and  $L/M$  distributions may point toward evolutionary effects, i.e., whether some RQ sources may be the parent population for all quasars (for example, NLSy1s, “extreme Pop. A” sources, may evolve into Pop. B RQ or even RL depending on accretion of angular momentum and/or host galaxy type/evolution).

In the future we will need of an orientation indicator for each individual AGN. This is very important for a correct evaluation of  $M$ . The  $CIV\lambda 1549$  line profile shows promise as an orientation indicator at least for Pop. A sources (Richards et al. 2002). It may also provide us with important clues about aspects of Broad Line Region structure and its dependence on  $L/M$ , and ultimately, with a 3D observational space to uniquely map into a 3D “physical” parameter space defined by  $M$ ,  $L/M$  and orientation.

## ACKNOWLEDGMENTS

The authors acknowledge support from the Italian Ministry of University and Scientific and Technological Research (MURST) through grant Cofin 00–02–004. We also wish to thank Giovanna Stirpe for fruitful discussions and a careful reading of the manuscript. This research has made use of the NASA/IPAC Extragalactic Database (NED) which is operated by the Jet Propulsion Laboratory, California Institute of Technology, under contract with the National Aeronautics and Space Administration.

## REFERENCES

- Boroson T., 2002, ApJ 565, 78  
 Boroson T.A., Green R.F., 1992, ApJS 80, 109  
 Boroson, T. A., Persson, S. E., & Oke, J. B. 1985, ApJ, 293, 120  
 Bongardo C., Zamanov R., Marziani P., Calvani M., Sulentic J. W., 2002, in AGN5: Inflows, Outflows and Reprocessing around Black Holes, [www.unico.it/ilaria/AGN5/proceedings.html](http://www.unico.it/ilaria/AGN5/proceedings.html) (astro-ph/0211418)  
 Brotherton, M. S., 1996, ApJS 102, 1  
 Collin, S., Boisson, C., Mouchet, M., Dumont, A.-M., Coupé, S., Porquet, D., Rokaki, E., 2002, A&A 388, 771  
 Dultzin-Hacyan, D., Marziani, P., & Sulentic, J. W. 2000, Revista Mexicana de Astronomia y Astrofisica Conference Series, 9, 308  
 Efron B., Tibshirani R.J., 1993, An introduction to the Bootstrap, Monographs on Statistics and applied Probability vol.57, Chapman & Hall, New York  
 Elvis, M., Wilkes, B. J., McDowell, J.C., Green, R. F., Bechtold, J., Willner, S. P., Oey, M. S., Polomski, E.; Cutri, R., 1994, ApJS 95, 1  
 Fabian A.C., 1999, MNRAS 308, L39  
 Falcke, H., Patnaik, A.R., Sherwood, W., 1996, ApJ, 473, L13  
 Ferland, G. J. 2000, Revista Mexicana de Astronomia y Astrofisica Conference Series, 9, 153  
 Gaskell, C. M., Brandt, W. N., Dietrich, M., Dultzin-Hacyan, D., & Eracleous, M. 1999, ASP Conf. Ser. 175: Structure and Kinematics of Quasar Broad Line Regions, Granato, G. L., Silva, L., Monaco, P., Panuzzo, P., Salucci, P., De Zotti, G., & Danese, L. 2001, MNRAS, 324, 757  
 Grupe, D., Beuermann, K., Mannheim, K., Thomas, H.-C., 1999, A&A 350, 805  
 Grupe, D., Leighly, K. M., Thomas, H.-C., Laurent-Muehleisen, S. A., 2000, A&A 356, 11  
 Jarvis, M. J., McLure, R. J., 2002, MNRAS 336, 38  
 Ho, L. C., 2002, ApJ 564, 120  
 Kaspi S., Smith P.S., Netzer H., Maoz D., Jannuzi B.T., Giveon U., 2000, ApJ 533, 631  
 Kollatschny W., Bischoff K., 2002, A&A, 386, 19  
 Krongold, Y., Dultzin-Hacyan, D., & Marziani, P. 2001, AJ, 121, 702  
 La Franca, F., Gregorini, L., Cristiani, S., de Rutter, H., & Owen, F. 1994, AJ, 108, 1548  
 Lacy, M., Laurent-Muehleisen, S. A., Ridgway, S. E., Becker, R.H., White, R. L., 2001, ApJ 551, L17  
 Laor A., 2000, ApJ 543, L111

- Malkan, M. A. & Moore, R. L. 1986, ApJ, 300, 216  
Mathur, S., 2000, NewAR 44, 469  
Mathur S., Kuraszkiwicz, J., Czerny B., 2001, NewA 6, 321  
Marziani, P., Sulentic, J. W., Dultzin-Hacyan, D., Calvani, M., Moles, M., 1996, ApJS 104, 37  
Marziani P., Sulentic J.W., Zamanov R., Calvani M., Dultzin-Hacyan D., Bachev R., Zwitter T., 2003b, ApJS, in press (M03)  
Marziani, P., Zamanov, R., Sulentic, J. W., Calvani, M., & Dultzin-Hacyan, D. 2003a, MemSAIt, 74, 492  
McLure, R. J., Kukula, M. J., Dunlop, J. S., Baum, S. A., O'Dea, C. P., & Hughes, D. H. 1999, MNRAS, 308, 377  
Murray, N., Chiang, J., Grossman, S. A., & Voit, G. M. 1995, ApJ, 451, 498  
Nicastro, F. 2000, ApJL, 530, L65  
Nicastro, F., Martocchia, A., & Matt, G. 2003, ApJL, 589, L13  
Oshlack, A. Y. K. N., Webster, R. L., & Whiting, M. T. 2002, ApJ, 576, 81  
Schlegel D. J., Finkbeiner D. P., & Davis M., 1998, ApJ 500, 525  
Sulentic J.W., Marziani P., & Dultzin-Hacyan D., 2000a, AR A&A, 38, 521  
Sulentic, J. W., Zwitter, T., Marziani, P., & Dultzin-Hacyan, D. 2000b, ApJ, 536, L5  
Sulentic, J. W., Marziani, P., Zamanov, R., Bachev, R., Calvani, M., Dultzin-Hacyan, D., 2002 ApJ, 566, L71  
Sulentic, J. W., S. Zamfir, Marziani, P., Bachev, R., Calvani, M., Dultzin-Hacyan, D., 2003 ApJL, submitted  
Véron-Cetty M.-P., & Véron P., 2001, A & A 374, 92  
Véron-Cetty M.-P., Véron P., Gonçalves A.C., 2001, A & A 372, 730  
Véron P., Gonçalves A.C., Véron-Cetty M.-P., 2002, A & A 384, 826  
Vestergaard, M., 2002, ApJ 571, 733  
Williams, R. J., Pogge, R. W., & Mathur, S. 2002, AJ, 124, 3042  
Wilman, R. J., Johnstone, R. M., Crawford, C. S., 2000, MNRAS, 317, 9  
Wilson, A. S. & Colbert, E. J. M. 1995, ApJ, 438, 62  
Woo J.-H., Urry C.M., 2002a, ApJ 579, 530  
Woo J.-H., Urry C.M., 2002b, ApJ 581, L5  
Wandel, A., Peterson, B. M., Malkan, M. A., 1999, ApJ 526, 579  
Zamanov, R. & Marziani, P. 2002, ApJL, 571, L77  
Zamanov R., Marziani P., Sulentic J.W., Calvani M., Dultzin-Hacyan D., Bachev R., 2002, ApJ 576, 9  
Zheng X. Z., Xia X. Y., Mao S., Wu H., Deng Z. G., 2002, AJ 124, 18